

# The dependence of halo bias on the protohalo shape alignment with the initial tidal field

Jounghun Lee <sup>a,1</sup> Jun-Sung Moon <sup>a,b</sup>

<sup>a</sup>Department of Physics and Astronomy, Seoul National University,  
Kwanak-ro 1, Kwanak-gu, Seoul 08826, Republic of Korea

<sup>b</sup>Research Institute of Basic Sciences, Seoul National University,  
Kwanak-ro 1, Kwanak-gu, Seoul 08826, Republic of Korea

E-mail: [cosmos.hun@gmail.com](mailto:cosmos.hun@gmail.com), [jsmoon.astro@gmail.com](mailto:jsmoon.astro@gmail.com)

**Abstract.** We present a numerical evidence supporting the primordial origin of secondary halo bias even on the galactic mass scale. Analyzing the data from the TNG 300-1 simulations, we investigate the dependence of halo bias on the degree of misalignment between the protohalo inertia and initial tidal tensors,  $\tau$ , measured at redshift,  $z_i = 127$ . From the TNG 300-1 galactic halos in logarithmic mass range of  $10.5 < m \equiv \log[M/(h^{-1}M_\odot)] \leq 13$  identified at  $z = 0, 0.5$  and  $1$ , a clear signal of  $\tau$  bias is detected. For the case that  $\tau$  is measured from the initial tidal field smoothed on the scale of  $R_f/(h^{-1}\text{Mpc}) \lesssim 1$ , the halo  $\tau$  bias is found to be very similar in its tendency and amplitude to the spin bias at all of the three redshifts, if the effects of backsplash halos are properly eliminated. For the case of  $R_f/(h^{-1}\text{Mpc}) = 2$ , the  $\tau$  bias at  $z = 1$  turns out to behave like the age bias, diminishing rapidly in the range of  $m > 12$ . At  $z = 0$  and  $0.5$ , however, the  $\tau$  and age bias factors show large differences in their overall strengths, which is attributed to the dominant nonlinear effects that undermine the former but enhance the latter. Given these numerical results along with the previous finding [1] that  $\tau$  shares a large amount of mutual information with the formation epochs and spin parameters of galactic halos, it is concluded that the origins of halo age and spin bias must be closely linked with the primordial factor,  $\tau$ , and that the difference in the tendency between the two bias factors on the galactic mass scale reflects the multi-scale influence of  $\tau$  on the halo secondary properties.

---

<sup>1</sup>Corresponding author.

---

## Contents

<b>1</b>	<b>Introduction</b>	<b>1</b>
<b>2</b>	<b>Detection of halo <math>\tau</math> bias and its implication on the secondary bias</b>	<b>2</b>
2.1	A brief review of halo age and spin bias trends	2
2.2	Scale and redshift dependence of halo $\tau$ -bias	7
<b>3</b>	<b>Summary and conclusion</b>	<b>12</b>

---

## 1 Introduction

The dark matter halos are biased tracers of the underlying dark matter (DM) particles, as the former exhibits mass-dependent difference in their clustering strengths from the latter [2, 3]. The halos with mass  $M$  higher than the characteristic mass scale  $M_*$  tend to cluster more strongly than the DM particles, while the opposite tendency is exhibited by the low-mass counterparts with  $M \lesssim M_*$ . Here,  $M_*$  satisfies the condition of  $\sigma(M_*) = \delta_c$  with critical density contrast for collapse,  $\delta_c$ , and rms density fluctuation,  $\sigma$  [4]. This mass dependence of halo bias is predicted by the standard excursion set theory [3, 5, 6], which effectively describes the growths of initial density peaks till their gravitational collapse as random walking processes.

It was, however, discovered by multiple N-body simulations that the halo bias depends not only on mass but also on secondary properties like formation epoch, concentration, sub-structure abundance, velocity anisotropy, potential depth, accretion rate, shape and spin parameter as well [7–27]. Among these secondary properties, what turned out to exhibit the strongest bias signal is the halo age for which the formation epoch and concentration parameter often stand proxy [7, 9, 14, 19–21]. In the lowest-mass section ( $M \ll M_*$ ) is found a positive age bias trend that the older halos cluster more strongly. While in the highest-mass section ( $M \gg M_*$ ) is detected the opposite tendency that the younger halos cluster more strongly, i.e., negative age bias. The inversion from negative to positive age bias trend was witnessed around the characteristic mass scale  $M_*$  [21]. Regarding the other secondary properties, their bias trends were shown to be similar to that of the halo ages, except for the spin bias, which inverts at a much lower mass threshold  $M \ll M_*$  [19–21, 28].

Ever since the first discovery of this phenomenon [7], much theoretical effort was made to physically understand why the DM halos with different secondary properties cluster differently. Although no standard theory has yet to be fully established, it was conventionally accepted that the secondary bias of low-mass halos differs in its origin from that of high-mass counterparts. In the highest-mass section ( $M \gg M_*$ ), the secondary halo bias was shown by ref. [29] to have a primordial origin. Incorporating the peak curvature dependence of initial density correlations into the excursion set theory, ref. [29] analytically proved that the Lagrangian halo bias factor in the asymptotic limit of  $M \gg M_*$  is a function of the curvature of initial density peaks, on which the halo formation epochs depend.

Whereas, in the lowest-mass section ( $M \ll M_*$ ), the secondary bias was often attributed to the nonlinear physical processes during their assembly histories. Ref. [23] scrupulously examined various theories suggested by the previous works for the origin of low-mass age bias and found that the following three mechanisms should make the most significant contributions:

first, the presence of backplash halos in the vicinity of their former higher-mass hosts [14, 28, 30]; second, the effects of large-scale web environments which can differentiate the formation epochs of halos at fixed mass by either facilitating or impeding mass accretion [15]; third, the shock heat generated during the collapse of largest-scale structures, which can slow down the mass accretion into the filament and sheet halos [29, 31].

In the analysis of ref. [23], however, it was also found that when the backplash halos were excluded, the fraction of low-mass halos yielding positive age bias was quite low, which implied that not only the highest-mass halos but also the lower mass halos may have had negative age bias of primordial origin until they were vulnerably exposed to the aforementioned physical mechanisms. This idea, *the primordial origin of secondary halo bias* on the lower-mass scale of  $M \lesssim M_*$ , was also supported by the result of ref. [24] that the secondary halo properties are more strongly correlated with the linear density field rather than with the evolved density field. According to ref. [24], the secondary halo bias should be a collateral byproduct of the multi-scale competition between the external and internal correlations of secondary halo properties with the linear density field, where the external and internal correlations are measured on the scales larger and smaller than the Lagrangian halo radius, respectively. In these previous works, however, it was still inconclusive which primordial factor actually drives the halo bias to acquire dependence on the secondary properties even on the mass scale of  $M \lesssim M_*$ , and what causes the age and spin bias to behave differently on this mass scale [20, 21, 28], if both of them share the same origin [13, 20].

For the verification of the primordial origin of the secondary bias of lower mass halos, it is necessary to find out a primordial factor on which the lower-mass halo bias exhibits the same strength of dependence as (or at least similar to) on the other secondary properties. In addition, a proper explanation for the difference between the age and spin bias in terms of this singled out primordial factor is also required. In light of our prior work where the ages and spins of galactic halos were found to share a large amount of mutual information with the degree of misalignments,  $\tau$ , between the principal axes of protohalo inertia and initial tidal tensors, we put forth a conjecture that  $\tau$  may be the primordial factor, and attempt to verify this conjecture by exploring the halo  $\tau$  bias. As in ref. [23], we will focus on the galactic mass scale,  $10.5 < m \equiv \log [M/(h^{-1} M_\odot)] \leq 13$ , where the existence of the secondary bias of primordial origin remains a crux, and the trend of spin bias significantly deviates from that of age bias [19–21, 28].

The outlines of the upcoming sections are as follows. In section 2.1, the halo age and spin bias factors are reviewed, and their mutual differences on the galactic mass scales are reinspected. In section 2.2, the dependence of the halo bias on the primordial factor  $\tau$  and the variation of its strength with mass and redshift are investigated, and compared with those of the halo age and spin bias. In section 3, the key results are summarized and their physical implications are discussed.

## 2 Detection of halo $\tau$ bias and its implication on the secondary bias

### 2.1 A brief review of halo age and spin bias trends

To numerically explore if the secondary halo bias has a primordial origin even on the galactic mass scale of  $10.5 < m \leq 13$ , we utilize the data from the 300 Mpc volume run (TNG300-1) of the IllustrisTNG suite of cosmological gravo-magneto-hydrodynamical simulations [32–37]. The TNG 300-1 run was conducted on a box of volume  $V_{\text{tot}} \equiv (205)^3 h^{-3} \text{Mpc}^3$  with the Planck initial condition [38] to track the dynamical evolution of  $2 \times 2500^3$  particles from the

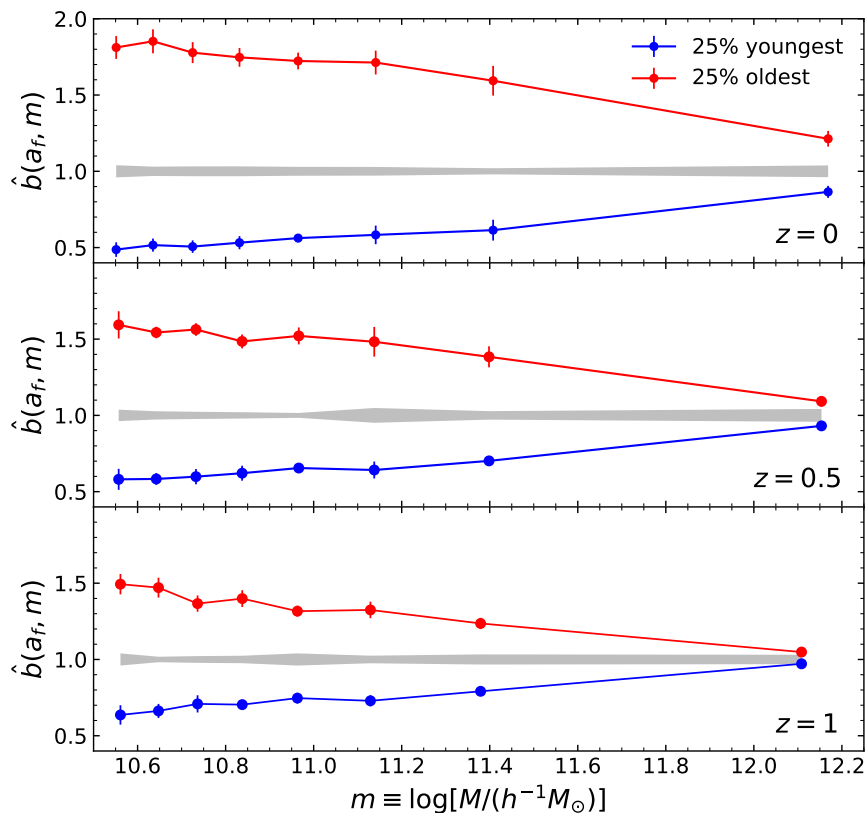


**Figure 1.** Relative age bias,  $\hat{b}(a_f, m)$ , from the 8  $m$ -selected subsamples of the galactic halos belonging to the top (red filled circles) and bottom (blue filled circles) quartiles of their ages versus the mean value of  $m$  averaged over each  $m$ -selected subsample, at three different redshifts. In each panel, the horizontal grey filled area represents the  $1\sigma_b$  Jackknife scatter around the relative halo bias  $\hat{b}(m)$  from the whole population of the galactic halos in the logarithmic mass range of  $10.5 \leq m \leq 13$ .

initial state  $z_i = 127$  down to the present epoch  $z = 0$ . One half of the particles in the TNG 300-1 are baryonic cells with individual mass of  $1.1 \times 10^7 M_\odot$ , while the other half are collisionless DM particles each of which is as massive as  $5.9 \times 10^7 M_\odot$ . The standard friends-of-friends (FoF) with the linkage length parameter of 0.2 and SUBFIND algorithms [39] were employed to resolve the bound halos and their substructures, respectively, in the TNG 300-1 snapshots [34]. Selecting the most massive central subhalos of the FoF groups, we extract information on their comoving positions ( $\mathbf{x}$ ), total masses ( $M$ ), formation epochs ( $a_f$ ) as defined in ref. [40, 41] and spin parameters ( $\lambda$ ) as defined in ref. [42] from the publicly released dataset of the TNG 300-1 simulations<sup>1</sup>. Throughout this paper, we will refer to the selected central subhalos as *galactic halos*, and consider only two secondary properties,  $a_f$  and  $\lambda$ , of them.

The Eulerian bias factor of dark halos,  $b(m)$ , at a given redshift is defined as  $b(m) \equiv$

<sup>1</sup><https://www.tng-project.org/data/>

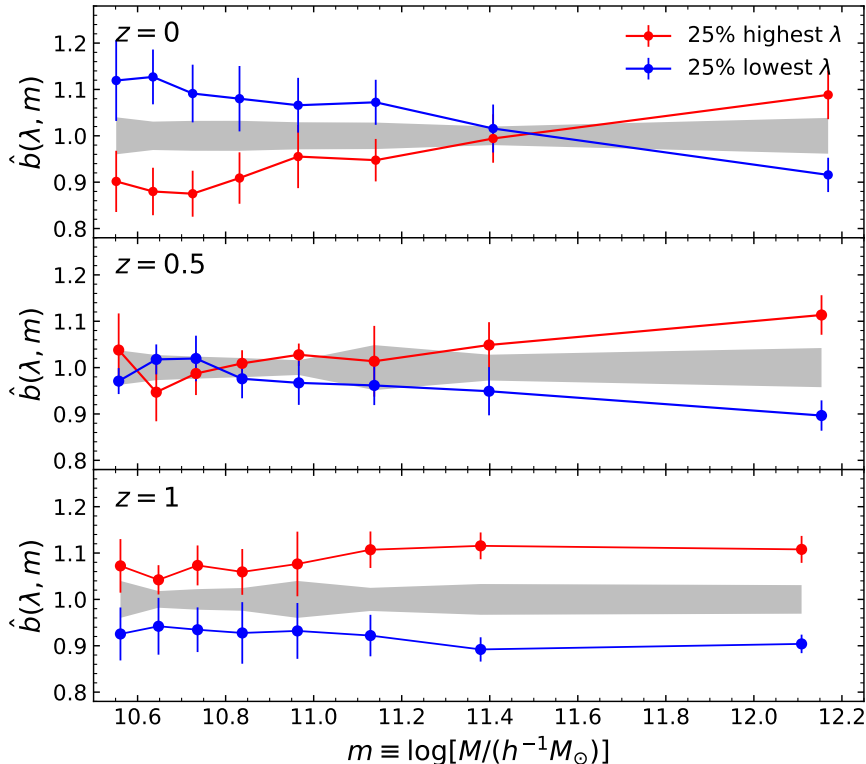


**Figure 2.** Relative spin bias from the top (red filled circles) and bottom (blue filled circles) quartiles of the halo spin parameters.  $\lambda$ .

$\delta_h(m)/\delta$  where  $\delta_h(m)$  is the number density contrast of the halos with logarithmic masses in a differential interval of  $[m, m + dm]$  within an overdense region of Eulerian volume  $\Delta V$  [3], while  $\delta$  is the matter density contrast within  $\Delta V$ . Applying the extended excursion set theory, ref. [3] evaluated  $\delta_h(m)$  as

$$\delta_h(m) \equiv \frac{n(m|\delta > 0)}{n(m)\Delta V} - 1, \quad (2.1)$$

where  $n(m)$  is the unconditional mass function of halos observed at  $z$ , while  $n(m|\delta > 0)$  is the conditional mass function of those halos embedded in  $\Delta V$ . In the asymptotic limit where  $\Delta V$  is much larger than the volumes of individual halos with logarithmic mass  $m$ ,  $b(m)$  is called the Eulerian *linear* bias factor and shown to be equal to the Lagrangian bias plus unity [3]. Throughout this paper, we will focus on the Eulerian linear bias and its dependence on the halo secondary properties.

The following flow chart describes how we determine the relative age and spin bias factors from the TNG 300-1 data in accordance with eq.(2.1):

1. Divide the simulation volume,  $V_{\text{tot}}$ , into  $64^3$  grids of equal volume  $\Delta V \equiv V_{\text{tot}}/(64^3)$ . This choice of grid number is made to ensure that  $b(m)$  is the *linear* bias factor. Given that the onset of nonlinear bias is witnessed on the scales below a typical cluster size

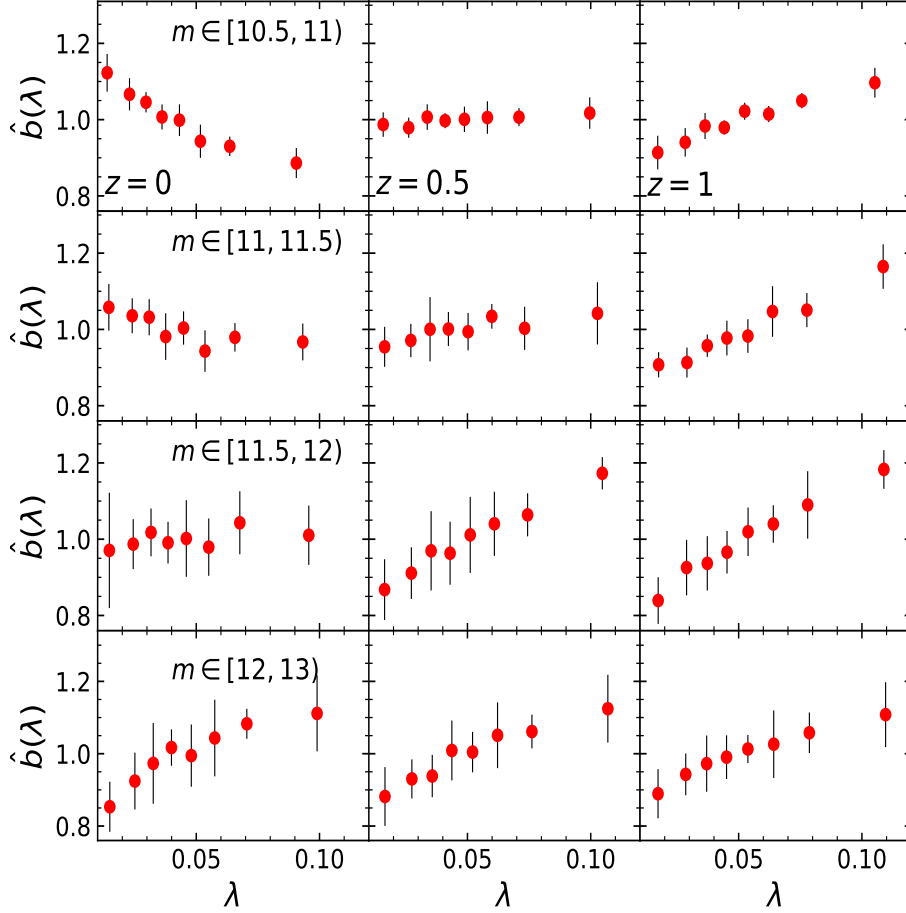


**Figure 3.** Relative spin in the whole range of  $\lambda$  (red filled circles) from the galactic halos belonging to four different  $m$ -bins at  $z = 0, 0.5$  and  $1$ .

$\sim 2 h^{-1} \text{Mpc}$  [43], the evaluation of a linear bias factor requires  $\Delta V > (2 h^{-1} \text{Mpc})^3$ . The grid number,  $64^3$ , satisfies this condition and simultaneously allows us to avoid poor number statistics in the evaluation of secondary bias, which can be caused when grid number is too small.

2. Construct the matter density contrast field,  $\delta$ , on the grids by applying the cloud-in-cell algorithm to the particle snapshot at each of the three redshifts, and select the galactic halos in the logarithmic mass range of  $10.5 < m \equiv \ln[M/(h^{-1} M_{\odot})] \leq 13$  to make a main sample.
3. Split the main sample into eight subsamples of equal size according to the values of  $m$ . Treat the galactic halos belonging to each  $m$ -selected subsample as particles, construct the halo number density contrast field,  $\delta_h(m)$ , with the help of the cloud-in-cell method.

4. Examine the  $\delta$  value at each of  $64^3$  grids and select those grids at which  $\delta \geq \sigma$  to minimize the shot noise. Take the ratio,  $\delta_h(m)/\delta$ , at each of the selected grids, and determine  $b(m)$  as the ensemble average of this ratio over the selected grids for each of the 8  $m$ -selected subsamples.
5. Create eight jackknife resamples by dividing the selected grids points according to the grid locations, and compute the Jackknife errors from the eight resamples (one standard deviation scatter of the bias factor obtained from each resample from the original  $b(m)$  obtained over  $V_{\text{tot}}$ ).
6. Repeating the above steps (2)-(5), but with only those youngest (oldest) galactic halos whose formation epochs belong to the top (bottom) quartile values of  $a_f$ , determine the halo age bias,  $b(a_f, m)$ , and take its ratio to  $b(m)$  to obtain the relative age bias,  $\hat{b}(a_f, m) \equiv b(a_f, m)/b(m)$ .
7. Repeating the above steps (2)-(5), but with only those rapidly (slowly) spinning galactic halos whose spin parameters belong to the top (bottom) quartile of  $\lambda$ , determine the spin bias,  $b(\lambda, m)$  and then take its ratio to  $b(m)$  to obtain the relative spin bias,  $\hat{b}(\lambda, m) \equiv b(\lambda, m)/b(m)$ .

A total of 618777, 637406 and 644753 central subhalos are selected at  $z = 0, 0.5$  and 1, respectively. Figure 1 plots  $\hat{b}(a_f, m)$  versus the mean values of  $m$  of eight  $m$ -selected subsamples of the galactic halos with  $a_f$  belonging to its top and bottom quartiles (blue and red filled circles, respectively). As can be seen, our results are quite consistent with what was found in the previous works [7–9, 11, 16, 19–21], capturing two characteristic tendencies of the age bias: the older halos (25% lowest  $a_f$ ) cluster more strongly than the younger ones (25% highest  $a_f$ ) [21] and this age dependence of the halo bias becomes weaker at higher  $z$  [18]. Figure 2 plots the same as figure 2 but from the top and bottom quartiles of  $\lambda$ , confirming the existence of spin bias. As can be seen, the inversion from the negative to positive spin bias is witnessed around  $m \simeq 11.5$  only at  $z = 0$ . Meanwhile, at higher  $z$  the spin bias appears to become more significant as  $m$  increases in the mass range considered, showing no inversion. The overall trends of  $\hat{b}(a_f, m)$  and  $\hat{b}(\lambda, m)$  are all quite consistent with the previous findings [7–11, 14, 16, 19–21].

As can be seen, the spin bias is less significant than the age counterpart on the galactic mass scale. To see more closely how the halo bias changes with  $\lambda$  at each redshift, we split the main sample into four subsamples corresponding to the  $m$ -ranges of  $[10.5, 11)$ ,  $[11, 11.5)$ ,  $[11.5, 12)$  and  $[12, 13]$ . Dividing the range of  $\lambda$  of the galactic halos belonging to each of the four  $m$ -selected subsample into eight bins, we compute  $\hat{b}(\lambda)$  separately at each  $\lambda$  interval via the above flow chart. Figure 3 shows  $\hat{b}(\lambda)$  versus  $\lambda$  from the four  $m$ -selected subsamples at the three redshifts, revealing that the inversion of  $\hat{b}(\lambda)$  occurs not only in a  $m$ -dependent way but also in a  $z$ -dependent way. The galactic halos of mass  $10.5 \leq m \leq 11$  decreases (increases) with  $\lambda$  at  $z = 0$  ( $z = 1$ ), while at  $z = 0.5$ , they show little variation with  $\lambda$ .

It is worth mentioning here that we estimate the secondary halo bias by taking the excursion set approach based on eq. (2.1) rather than by employing the conventional methods based on the density correlations or power spectra [7, 9, 12, 19–21, 23]. True as it is that the conventional methods are quite efficient for the estimation of secondary halo bias in a wide mass range, it suffers from an ambiguity in the choice of the range of separation distance  $r$ , which may make it difficult to properly investigate the dependence of halo bias on a scale-dependent secondary property like  $\tau$ , the primary focus of the current analysis. Nevertheless,

our method turns out to reproduce quite well the overall trends of age and spin bias estimated by the conventional correlation function method in the galactic mass range.

## 2.2 Scale and redshift dependence of halo $\tau$ -bias

As mentioned in section 1, it was found by our prior work [1] that the basic traits of galactic halos share a large amount of mutual information with a primordial factor,  $\tau$ , defined as the degree of misalignment<sup>2</sup> between the principal axes of protohalo inertia and initial tidal tensors. For the case of massive galactic halos with  $m \geq 11.5$ , the primordial factor  $\tau$  was found to contain larger amounts of mutual information about the formation epochs and spin parameters than the halo mass, local density and environmental shears (see figure 3 in ref. [1]). Furthermore, the probability density functions of both of  $\lambda$  and  $\tau$  were also shown to be best approximated by the same Gamma distribution [1]. These prior results naturally lead us to expect the existence of  $\tau$  bias and to speculate its possible links with the age and spin bias.

In the following, we concisely describe the computational steps via which the relative  $\tau$  bias factor,  $\hat{b}(\tau, m)$ , is measured:

1. Trace back the constituent particles of each galactic halo back to the earliest epoch of redshift  $z_i = 127$  to find their Lagrangian positions,  $\mathbf{q} \equiv (q_i)$ , and their center of mass  $\mathbf{q}_c \equiv (q_{c,i})$ , as well. Then, compute the inertia tensor of a located protohalo,  $I_{jk}(\mathbf{q}_c)$ , as [1]

$$\hat{I}_{jk} \equiv \sum_{\mu=1}^{n_p} m_{\mu} (q_{\mu,j} - q_{c,j})(q_{\mu,k} - q_{c,k}), \quad (2.2)$$

where  $m_{\nu}$  is the mass of  $\nu$ th particle located at the initial position  $\mathbf{q}_{\mu} \equiv (q_{\mu,i})$ , and  $n_p$  is the number of the particles that constitute the protohalo.

2. Apply the cloud-in-cell method to the particle snapshot at redshift  $z_i = 127$  to determine the initial matter density contrast field,  $\delta(\mathbf{q})$ , on  $512^3$  grid points as in [1]. Find the Fourier space initial density contrast field,  $\delta(\mathbf{k})$ , via a Fast Fourier transformation (FFT) of  $\delta(\mathbf{q})$  with the Fourier space wave vector of  $\mathbf{k}$ .
3. Compute the Fourier space initial tidal field convolved by a Gaussian kernel with scale radius  $R_f$ , as  $\tilde{T}_{ij}(\mathbf{k}) \equiv k_i k_j \tilde{\delta}(\mathbf{k}) \exp(-|\mathbf{k}|^2 R_f^2/2)/|\mathbf{k}|^2$ . Then, perform an inverse FFT of it to obtain the real-space initial tidal field  $[T_{ij}(\mathbf{q})]$ . At the grid point in which  $\mathbf{q}_c$  falls, diagonalize  $T_{ij}(\mathbf{q}_c)$  to find its three orthonormal eigenvectors,  $\{\mathbf{e}_1, \mathbf{e}_2, \mathbf{e}_3\}$ .
4. Construct a rotation matrix,  $\mathbf{R}$ , whose three columns correspond to  $\{\mathbf{e}_1, \mathbf{e}_2, \mathbf{e}_3\}$ , and perform a similarity transformation of the protohalo inertia tensor as  $I'_{jk} = R_{jl}^{-1} I_{ls} R_{sk}$ .
5. For each galactic halo, compute the degree of misalignment,  $\tau(r_f)$ , between the principal axes of the protohalo inertia and initial tidal tensors smoothed on the scale of  $r_f \equiv R_f/(h^{-1}\text{Mpc})$  as [1]

$$\tau(r_f) \equiv \left[ \frac{(I'_{12})^2 + (I'_{23})^2 + (I'_{31})^2}{(I'_{11})^2 + (I'_{22})^2 + (I'_{33})^2} \right]^{1/2}. \quad (2.3)$$

<sup>2</sup>Since the principal axes of a protohalo inertia tensor are aligned with its shape axes, it is equivalent to saying that  $\tau$  describes how weakly the protohalo shape axes are anti-aligned with the principal axes of the initial tidal field.



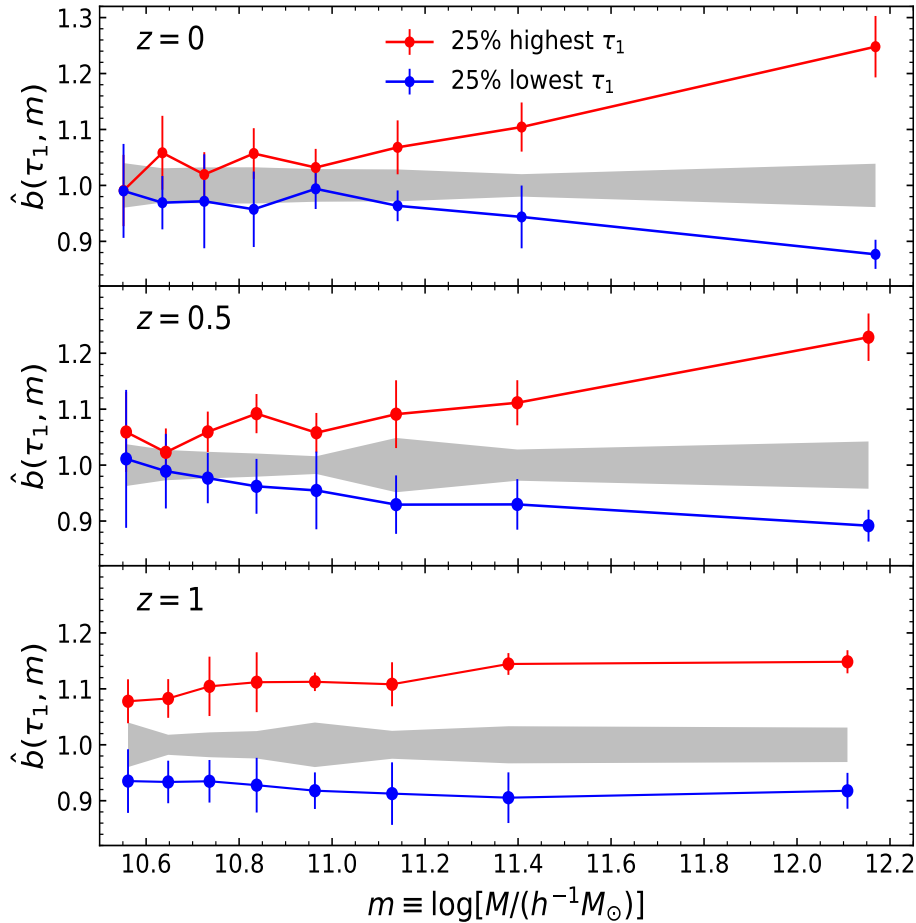


**Figure 4.** Relative  $\tau_1$  bias from the galactic halos whose primordial  $\tau_1$  values belong to the top (red filled circles) and bottom (blue filled circles) quartiles, where  $\tau_1$  quantifies how weakly the triaxial proto-halos shapes are aligned with the principal axes of the initial tidal field smoothed on the scale of  $R_f/(h^{-1}\text{Mpc}) = 1$  (see eq.(2.2)). Note a robust similarity between  $\hat{b}(\tau_1, m)$  and  $\hat{b}(\lambda, m)$  (see figure 2) at  $z = 1$ .

6. Follow the flow chart described in section 2.1 to obtain the relative  $\tau$  bias factor for three different cases of  $r_f = 0.5, 1$  and  $2$ , denoted by  $\hat{b}(\tau_{0.5}, m)$ ,  $\hat{b}(\tau_1, m)$  and  $\hat{b}(\tau_2, m)$ , at each redshift.

Figure 4 shows the relative  $\tau_1$  bias, revealing how  $\hat{b}(\tau_1, m)$  behaves as  $m$  changes at different redshifts. The factor by which  $\hat{b}(\tau_1, m \gtrsim 12)$  enhances as  $\tau_1$  changes from the bottom to top quartile reaches up to  $\sim 1.4$  at  $z = 0$  but slightly diminishes down to  $\sim 1.3$  at  $z = 1$ . In the lower mass range of  $m \leq 11.5$ , the relative  $\tau_1$  bias has insignificantly low values at  $z = 0$  but tends to become significant as  $z$  increases. The overall trend is that the  $\tau_1$  bias mildly increases as  $m$  increases at all of the three redshifts. Note that the behavior and amplitude of  $\hat{b}(\tau_1, m)$  at  $z = 1$  is quite similar to that of  $\hat{b}(\lambda, m)$  shown in figure 2. But,

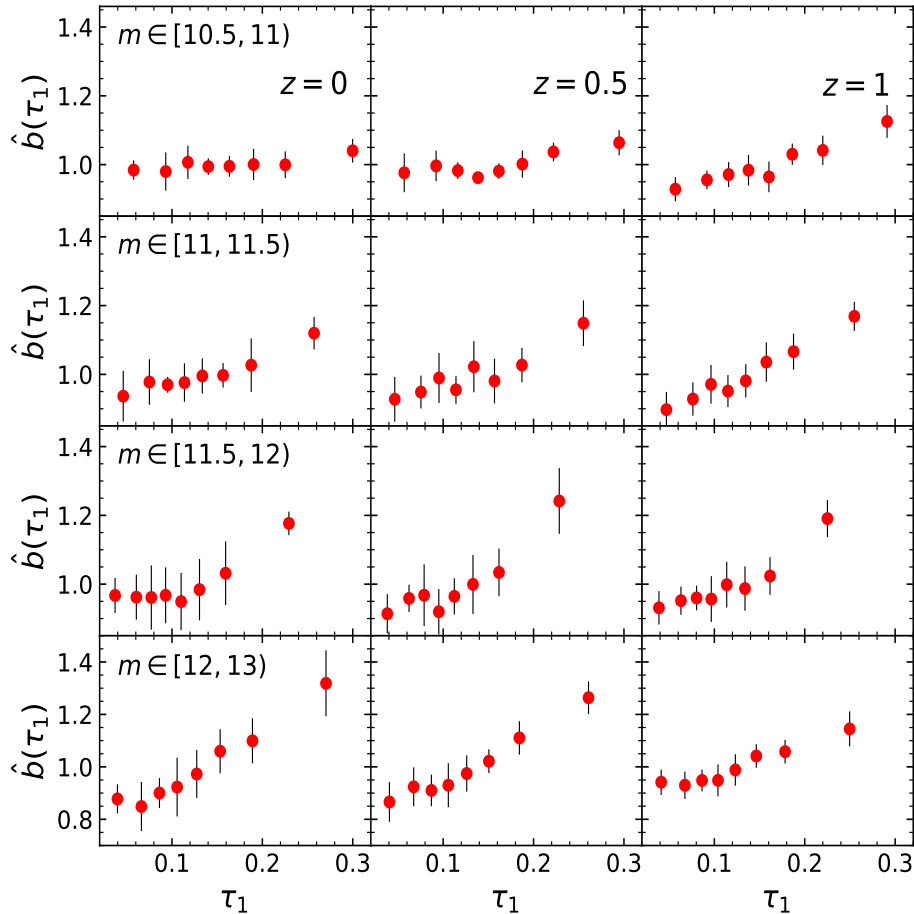


**Figure 5.** Relative  $\tau_1$  in the whole range of  $\tau_1$  (red filled circles) from the galactic halos belonging to four different  $m$ -bins at  $z = 0, 0.5$  and  $1$ .

at  $z = 0.5$  and  $0$ , a notable difference exists between  $\hat{b}(\tau_1, m)$  and  $\hat{b}(\lambda, m)$  especially in the low mass range  $m \leq 11.5$ . Unlike  $\hat{b}(\lambda, m)$ , no inversion to the negative bias at  $m \simeq 11.5$  is exhibited by  $\hat{b}(\tau, m)$  at  $z = 0$ .

As mentioned in section 1, however, it was already proved by ref. [28] that the inversion of  $\hat{b}(\lambda, m \simeq 11.5)$  at  $z \simeq 0$  was entirely due to the locations of abundant backsplash halos in the vicinity of massive former hosts. When the backsplash halos were properly excluded from the calculation of  $\hat{b}(\lambda, m)$  at  $z = 0$ , the inversion signal disappeared even at  $z = 0$ . What ref. [28] also found that at  $z \geq 1$  the effect of backsplash halos on  $\hat{b}(\lambda, m)$  was negligible, since the abundance of backsplash halos decreases sharply with the increment of  $z$ . Comparing  $\hat{b}(\tau_1, m)$  with the results of ref. [28], i.e.,  $\hat{b}(\lambda, m)$  measured after the elimination of backsplash halos (see figure 3 in ref. [28]), we note that a robust similarity between the spin and  $\tau_1$  bias factors exists even at  $z = 0$ .

To gain a better insight on the dependence of halo bias on  $\tau_1$  at each redshift, we

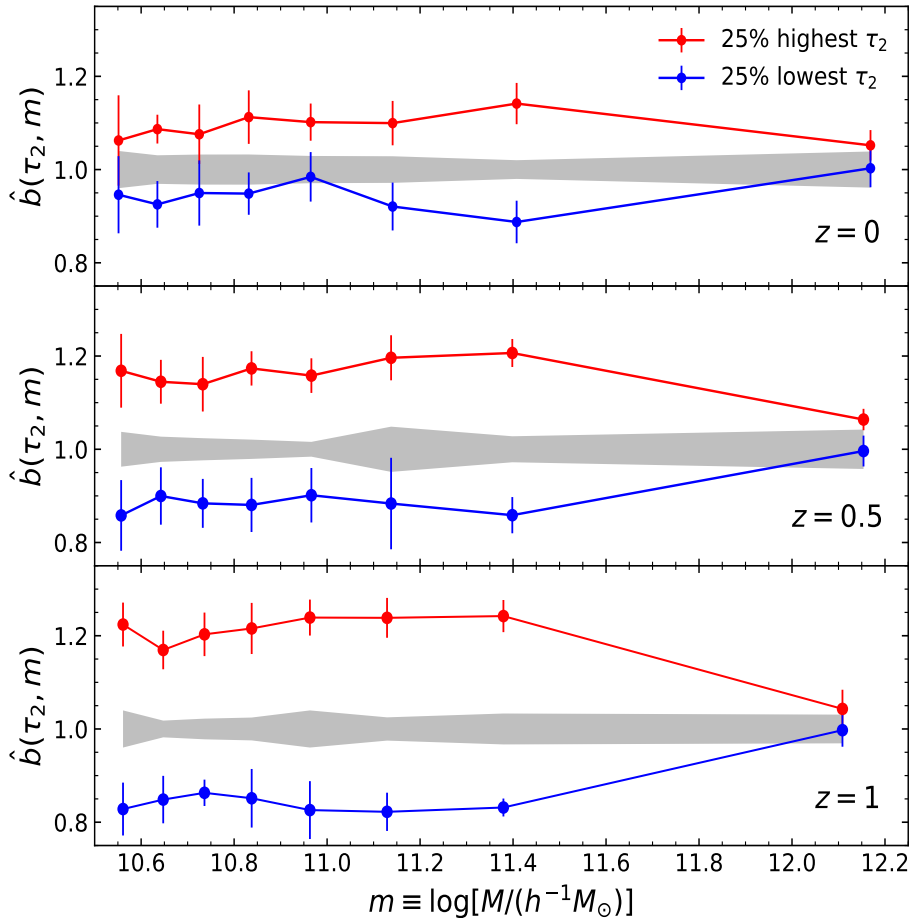


**Figure 6.** Same as figure 4 but for the case of  $\tau_2$  that quantifies how weakly the triaxial shapes of protohalos are aligned with the principal axes of the initial tidal field smoothed on the larger scale,  $R_f/(h^{-1}\text{Mpc}) = 2$ . Note a similarity between the relative  $\tau_2$  and  $a_f$  bias (see figure 1) at  $z = 1$ .

also compute  $\hat{b}(\tau_1)$  separately from the four  $m$ -selected subsamples by following the same procedure used to measure  $\hat{b}(\lambda)$  in section 2.1. Figure 5 shows the same as figure 3 but with  $\tau_1$  substituting for  $\lambda$ . The comparison with figure 3 reveals that at  $z = 0.5$  and 1, the overall trends of  $\hat{b}(\tau_1)$  and  $\hat{b}(\lambda)$  are indeed quite similar to each other not only in the top and bottom quartiles but also in the whole ranges of  $\tau_1$  and  $\lambda$ . Note that even at  $z = 0$  where the effects of backplash halos are dominant the two bias factors show similar behaviors in the range of  $12 \leq m \leq 13$ .

To see how the relative  $\tau$  bias changes with the smoothing scale  $r_f$ , we repeat the whole analysis but for the case of  $r_f = 2$  and 0.5. Figure 6 plots the same as figure 4 but for the case of  $r_f = 2$ , revealing a striking difference in the behavior of  $\hat{b}(\tau_2, m)$  from that of  $\hat{b}(\tau_1, m)$ . In contrast to  $\hat{b}(\tau_1, m)$ , a mild decrease of  $\hat{b}(\tau_2, m)$  with the increment of  $m$  is found in the whole mass range considered. Note that at  $z = 1$  the overall trend of the relative  $\tau_2$  bias is quite

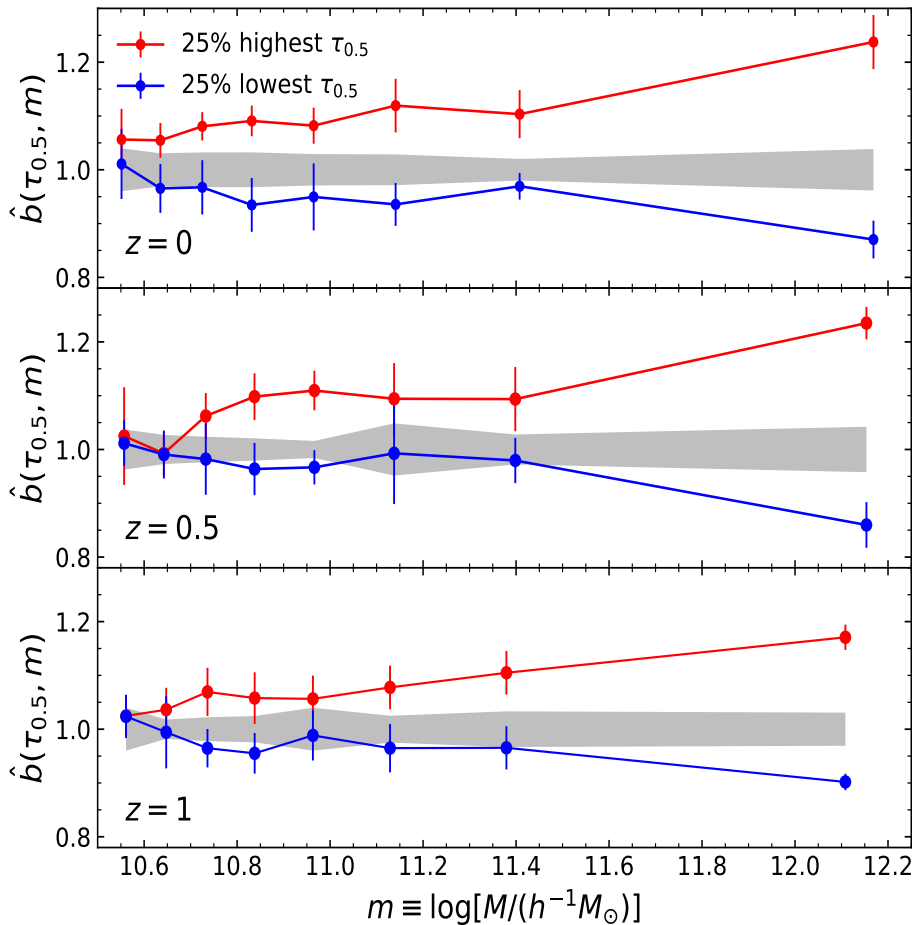


**Figure 7.** Same as figure 4 but for the case of  $\tau_{0.5}$  that quantifies how weakly the triaxial shapes of protohalos are aligned with the principal axes of the initial tidal field smoothed on the smaller scale,  $R_f/(h^{-1}\text{Mpc}) = 0.5$ .

similar to the relative age bias shown in figure 1. Recalling the results of [23] that the three nonlinear mechanisms had an effect of deviating the halo age bias from the primordial trend by augmenting it especially in the low-mass range ( $m \lesssim 12.5$ ), we interpret the similarity between  $\hat{b}(\tau_2, m)$  and  $\hat{b}(a_f, m)$  at  $z = 1$  as an evidence supporting the primordial origin of the halo age bias [23, 24]. We also take the low  $\tau_2$  bias signal at  $z = 0$  as a result indicating that the three nonlinear processes undermines the  $\tau_2$  bias at low redshift, deviating further  $\hat{b}(\tau_2, m)$  from  $\hat{b}(a_f, m)$ . In other words, while the halos undergo the three nonlinear processes, they tend to lose the primordially generated connections between  $\tau_2$  and  $a_f$ .

Figure 7 plots the same as figure 4 but for the case of  $r_f = 0.5$ . Although the  $\tau_{0.5}$  bias is similar in its overall trend to the  $\tau_1$  counterpart, the strength of the former seems to be significant even in the low-mass range of  $m \lesssim 11.5$  at  $z = 0$ , in contrast to the latter. The comparison of the results shown in figures 1-7 indicates that the behavior and strength of

$\tau(r_f)$  depends quite sensitively on  $r_f$  and that there is two characteristic scales, say  $r_a \simeq 2$  and  $r_s \simeq 1$ , on which the behaviors of  $\tau(r_f = r_a)$  and  $\tau(r_f = r_s)$  bias factors become quite similar to those of the spin and age bias, respectively, at  $z \simeq 1$ . Any departure of  $r_f$  from these characteristic scales in either direction cause  $\hat{b}(\tau)$  to behave differently from  $\hat{b}(a_f)$  and  $\hat{b}(\lambda)$ , respectively. We speculate that the primordial effect of  $\tau(r_f)$  on  $a_f$  and  $\lambda$  should be the strongest on these particular scales  $r_a$  and  $r_s$ , respectively. Moreover, given that  $r_a$  is larger than  $r_s$ , it can be inferred that  $a_f$  and  $\lambda$  are affected by the larger and smaller scale effects of  $\tau$  in the primordial epoch, respectively. In other words, the differences between the age and spin bias may be primordially caused by the multi-scale effects of  $\tau(r_f)$ . At lower redshifts  $z \lesssim 0.5$  when the secondary bias factors are severely modified by the nonlinear physical processes [23], however, the primordial  $\tau(r_f)$  effects seem to dwindle away especially in the low-mass range, no matter what  $r_f$  is.

### 3 Summary and conclusion

From the TNG 300-1 galactic halos in the mass range of  $10.5 < m \equiv \log[M/(h^{-1}M_\odot)] \leq 13$  at  $z = 0, 0.5$  and  $1$ , we have detected the significant dependence of halo bias on the primordial factors,  $\tau_{0.5}$ ,  $\tau_1$  and  $\tau_2$ , which denote the degree of misalignments of the triaxial protohalo shapes with the initial tidal tensors smoothed on the scales of  $r \equiv R_f/(h^{-1}\text{Mpc}) = 0.5, 1$  and  $2$ , respectively (see figures 4-7). Comparing the relative bias of the three primordial factors,  $\hat{b}(\tau_{0.5}, m)$ ,  $\hat{b}(\tau_1, m)$ , and  $\hat{b}(\tau_2, m)$ , with the relative age and spin bias,  $\hat{b}(a_f, m)$  and  $\hat{b}(\lambda, m)$  (see figures 1-2), we have found that at  $z = 1$ , the overall trend of  $\hat{b}(\tau_1, m)$ , is very similar to that of  $\hat{b}(\lambda, m)$  in the entire mass range considered. Although an apparent difference has been found between  $\hat{b}(\tau_1, m)$  and  $\hat{b}(\lambda, m)$  in the low-mass range ( $m \leq 11.5$ ) at  $z = 0$  and  $0.5$ , it has been realized that the exclusion of backplash halos fully recovers the robust similarity between them [28] even in the low-mass range of  $m \leq 11.5$  at all of the three redshifts.

It has also been found that  $\hat{b}(\tau_2, m)$  and  $\hat{b}(a_f, m)$  exhibit similar behaviors at  $z = 1$ , but evolve in opposite directions at lower redshifts: as  $z$  decreases, the former becoming weaker while the latter stronger. We have ascribed the deviation of  $\hat{b}(a_f, m)$  from  $\hat{b}(\tau_2, m)$  at  $z \leq 0.5$  to the three physical processes that ref. [23] already showed were mainly responsible for the age bias of low-mass halos at  $z = 0$ : the large-scale web environments, shock heats generated during the formation of large scale structures, and clustering of the backplash halos. These nonlinear processes seem to have two prolonged effects: diminishing the dependence of halo bias on the primordial factor,  $\tau_2$ , and enhancing the age bias of low-mass halos at lower redshifts.

It is interesting to see that only through the calculation of bias factors is found the difference between  $a_f$  and  $\lambda$  in the scale dependence of their correlations with  $\tau$ . In our prior work [1] where the respective correlations of these two properties with  $\tau$  were directly calculated on three different scales, the scatters around the mean values made it almost impossible to see whether or not their correlation strengths exhibit these variations with  $r_f$ . In other words, the similarities of  $\hat{b}(\tau_2)$  and  $\hat{b}(\tau_1)$  to  $\hat{b}(\lambda)$  and  $\hat{b}(a_f)$ , respectively, has led to this new discovery that the two halo properties,  $\lambda$  and  $a_f$ , are dominantly affected by the primordial spin factors defined on different scales.

We interpret  $\tau(r_f)$  as the protohalo response to the multi-scale influences of the initial tidal field,  $\mathbf{T}(r_f, z_i)$ . A higher (lower) value of  $\tau(r_f)$  corresponds to a slower (faster) response of a protohalo to  $\mathbf{T}(r_f, z_i)$ . If protohalos of same mass  $M$  respond more slowly (rapidly) to  $\mathbf{T}(r_f, z_i)$ , then they would be less (more) susceptible to its effect, which will eventually produce

a difference between them in their secondary properties linked with  $\mathbf{T}(r_f, z_i)$ . For the case of the spin parameter, it is produced under the primary influence of  $\mathbf{T}(r_f \simeq r_L, z_i)$  [44] where  $r_L \equiv [4M/(3\pi\bar{\rho})]^{1/3}$  is the Lagrangian virial radius of the protohalo [24]. Any difference in the response to  $\mathbf{T}(r_f \simeq r_L, z_i)$  would cause a difference in  $\lambda$  among the protohalos of same mass, originating the halo spin bias and its similarity to the  $\tau(r_f \simeq r_L)$  bias until the effects of backsplash halos modify the spin bias in the lower-mass range of  $m \leq 11.5$  at low redshifts. Whereas, for the case of the formation epochs, it is determined largely by  $\mathbf{T}(r_f > r_L, z)$  (i.e., the initial tidal effects on the scales larger than  $r_L$ ). If protohalos of same mass respond more slowly (rapidly) to  $\mathbf{T}(r_f > r_L, z)$  due to weak (strong) alignments of their shapes with  $\mathbf{T}(r_f > r_L, z)$ , then their formations will be delayed (expedited), which in turn will create the age bias similar to the  $\tau(r_f > r_L)$  bias. The memory for the primordial  $\tau(r_f > r_L)$  factor will be retained in the age bias until it is severely undermined by the nonlinear effects found by ref. [23].

Backing up the conjecture previously suggested by refs. [23, 24] that the secondary halo bias must have a primordial origin regardless of halo mass, the current work has made two new contributions. Firstly, we single out the primordial factor,  $\tau$ , the bias of which behaves like the age and spin bias on the galactic mass scale at  $z \simeq 1$ . Secondly, we have provided an explanation for the difference in behavior and tendency between the spin and age bias of galactic halos in terms of the primordial  $\tau$  factors defined on different scales. Our future work is in the direction of deriving an analytic model for the halo  $\tau$  bias in terms of linear quantities from the first principle, and exploring the  $\tau$  bias in a much wider range of mass.

## Acknowledgments

The IllustrisTNG simulations were undertaken with compute time awarded by the Gauss Centre for Supercomputing (GCS) under GCS Large-Scale Projects GCS-ILLU and GCS-DWAR on the GCS share of the supercomputer Hazel Hen at the High Performance Computing Center Stuttgart (HLRS), as well as on the machines of the Max Planck Computing and Data Facility (MPCDF) in Garching, Germany. JL acknowledges the support by Basic Science Research Program through the NRF of Korea funded by the Ministry of Education (No.2019R1A2C1083855). JSM acknowledges the support by the National Research Foundation (NRF) of Korea grant funded by the Korean government (MEST) (No. 2019R1A6A1A10073437).

## References

- [1] J. S. Moon and J. Lee, *Mutual information between galaxy properties and the initial predisposition*, JCAP **05** (2024) 111 doi:10.1088/1475-7516/2024/05/111 [arXiv:2311.03632 [astro-ph.CO]].
- [2] N. Kaiser, *On the spatial correlations of Abell clusters.*, Astrophys. J. **284** (1984) L9, doi:10.1086/184341
- [3] H. J. Mo and S. D. M. White, *An Analytic model for the spatial clustering of dark matter halos*, Mon. Not. Roy. Astron. Soc. **282** (1996) 347 doi:10.1093/mnras/282.2.347
- [4] J. E. Gunn and J. R. Gott, *On the Infall of Matter Into Clusters of Galaxies and Some Effects on Their Evolution.*, Astrophys. J. **176** (1972) 1 doi:10.1086/151605
- [5] W. H. Press and P. Schechter, *Formation of Galaxies and Clusters of Galaxies by Self-Similar Gravitational Condensation*, Astrophys. J. **187** (1974) 425 doi:10.1086/152650

- [6] J. R. Bond, S. Cole, G. Efstathiou and N. Kaiser, *Excursion set mass functions for hierarchical Gaussian fluctuations*, *Astrophys. J.* **379** (1991) 440 doi:10.1086/170520
- [7] L. Gao, V. Springel and S. D. M. White, *The Age dependence of halo clustering*, *Mon. Not. Roy. Astron. Soc.* **363** (2005) L66-L70, doi:10.1111/j.1745-3933.2005.00084.x [arXiv:astro-ph/0506510 [astro-ph]].
- [8] R. H. Wechsler, A. R. Zentner, J. S. Bullock and A. V. Kravtsov, *The dependence of halo clustering on halo formation history, concentration, and occupation*, *Astrophys. J.* **652** (2006), 71-84 doi:10.1086/507120 [arXiv:astro-ph/0512416 [astro-ph]].
- [9] L. Gao and S. D. M. White, *Assembly bias in the clustering of dark matter haloes*, *Mon. Not. Roy. Astron. Soc.* **377** (2007), L5, doi:10.1111/j.1745-3933.2007.00292.x, [arXiv:astro-ph/0611921 [astro-ph]].
- [10] Y. Li, H. J. Mo and L. Gao, *On Halo Formation Times and Assembly Bias*, *Mon. Not. Roy. Astron. Soc.* **389** (2008) 1419 doi:10.1111/j.1365-2966.2008.13667.x [arXiv:0803.2250 [astro-ph]].
- [11] O. Hahn, C. Porciani, A. Dekel and C. M. Carollo, *The Tidal Origin of the Environment Dependence of Halo Assembly*, *Mon. Not. Roy. Astron. Soc.* **398** (2009) 1742 doi:10.1111/j.1365-2966.2009.15271.x [arXiv:0803.4211 [astro-ph]].
- [12] A. Faltenbacher and S. D. M. White, *Assembly bias and the dynamical structure of dark matter halos*, *Astrophys. J.* **708** (2010), 469-473 doi:10.1088/0004-637X/708/1/469 [arXiv:0909.4302 [astro-ph.CO]].
- [13] I. Lacerna and N. Padilla, *The nature of assembly bias - II. Halo spin*, *Mon. Not. Roy. Astron. Soc.* **426** (2012) L26 doi:10.1111/j.1745-3933.2012.01316.x
- [14] R. Li, L. Gao, L. Xie and Q. Guo, *Assembly Bias of Dwarf-sized Dark Matter Haloes*, *Mon. Not. Roy. Astron. Soc.* **435** (2013), 3592 doi:10.1093/mnras/stt1551 [arXiv:1308.4204 [astro-ph.CO]].
- [15] M. Borzyszkowski, C. Porciani, E. Romano-Diaz and E. Garaldi, *ZOMG – I. How the cosmic web inhibits halo growth and generates assembly bias*, *Mon. Not. Roy. Astron. Soc.* **469** (2017) no.1, 594-611 doi:10.1093/mnras/stx873 [arXiv:1610.04231 [astro-ph.CO]].
- [16] T. Sunayama, A. P. Hearin, N. Padmanabhan and A. Leauthaud, *The Scale-Dependence of Halo Assembly Bias*, *Mon. Not. Roy. Astron. Soc.* **458** (2016) no.2, 1510-1516 doi:10.1093/mnras/stw332 [arXiv:1509.06417 [astro-ph.CO]].
- [17] T. Lazeyras, M. Musso and F. Schmidt, *Large-scale assembly bias of dark matter halos*, *JCAP* **03** (2017), 059 doi:10.1088/1475-7516/2017/03/059 [arXiv:1612.04360 [astro-ph.CO]].
- [18] S. Contreras, I. Zehavi, N. Padilla, C. Baugh, E. Jiménez and I. Lacerna, *The Evolution of Assembly Bias*, *Mon. Not. Roy. Astron. Soc.* **484** (2019) no.1, 1133-1148 doi:10.1093/mnras/stz018 [arXiv:1808.02896 [astro-ph.GA]].
- [19] A. N. Salcedo, A. H. Maller, A. A. Berlind, M. Sinha, C. K. McBride, P. S. Behroozi, R. H. Wechsler and D. H. Weinberg, *Spatial clustering of dark matter haloes: secondary bias, neighbour bias, and the influence of massive neighbours on halo properties*, *Mon. Not. Roy. Astron. Soc.* **475** (2018) 4411, doi:10.1093/mnras/sty109 [arXiv:1708.08451 [astro-ph.CO]].
- [20] J. W. Johnson, A. H. Maller, A. A. Berlind, M. Sinha and J. K. Holley-Bockelmann, *The Secondary Spin Bias of Dark Matter Haloes*, *Mon. Not. Roy. Astron. Soc.* **486** (2019) no.1, 1156-1166 doi:10.1093/mnras/stz942 [arXiv:1812.02206 [astro-ph.CO]].
- [21] G. Sato-Polito, A. D. Montero-Dorta, L. R. Abramo, F. Prada and A. Klypin, *The dependence of halo bias on age, concentration and spin*, *Mon. Not. Roy. Astron. Soc.* **487** (2019) 1570 doi:10.1093/mnras/stz1338 [arXiv:1810.02375 [astro-ph.GA]].

- [22] A. D. Montero-Dorta, M. C. Artale, L. R. Abramo, B. Tucci, N. Padilla, G. Sato-Polito, I. Lacerna, F. Rodriguez and R. E. Angulo, *The manifestation of secondary bias on the galaxy population from IllustrisTNG300*, Mon. Not. Roy. Astron. Soc. **496** (2020) no.2, 1182-1196 doi:10.1093/mnras/staa1624 [arXiv:2001.01739 [astro-ph.GA]].
- [23] P. Mansfield and A. V. Kravtsov, *The Three Causes of Low-Mass Assembly Bias*, Mon. Not. Roy. Astron. Soc. **493** (2020) no.4, 4763-4782 doi:10.1093/mnras/staa430 [arXiv:1902.00030 [astro-ph.CO]].
- [24] X. Wang, H. Wang, H. J. Mo, J. Shi and Y. Jing, *Evaluating the origins of the secondary bias based on the correlation of halo properties with the linear density field*, Astron. Astrophys. **654** (2021) A67 doi:10.1051/0004-6361/202141077 [arXiv:2104.10123 [astro-ph.CO]].
- [25] A. Balaguera-Antolínez, A. D. Montero-Dorta and G. Favole, *Secondary halo bias through cosmic time I: Scaling relations and the connection with the cosmic web*, [arXiv:2311.12991 [astro-ph.CO]].
- [26] A. D. Montero-Dorta and F. Rodriguez, *The dependence of assembly bias on the cosmic web*, [arXiv:2309.12401 [astro-ph.GA]].
- [27] J. M. Coloma-Nadal, F. S. Kitaura, J. E. García-Farieta, F. Sinigaglia, G. Favole and D. F. Sánchez, *The Hierarchical Cosmic Web and Assembly Bias*, [arXiv:2403.19337 [astro-ph.CO]].
- [28] B. Tucci, A. D. Montero-Dorta, L. R. Abramo, G. Sato-Polito and M. C. Artale, *The physical origins of low-mass spin bias*, Mon. Not. Roy. Astron. Soc. **500** (2020) no.3, 2777-2785 doi:10.1093/mnras/staa3319 [arXiv:2007.10366 [astro-ph.CO]].
- [29] N. Dalal, M. White, J. R. Bond and A. Shirokov, *Halo Assembly Bias in Hierarchical Structure Formation*, Astrophys. J. **687** (2008) 12-21 doi:10.1086/591512 [arXiv:0803.3453 [astro-ph]].
- [30] H. Wang, H. J. Mo and Y. P. Jing, *The distribution of ejected subhalos and its implication for halo assembly bias*, Mon. Not. Roy. Astron. Soc. **396** (2009) 2249 doi:10.1111/j.1365-2966.2009.14884.x [arXiv:0811.3558 [astro-ph]].
- [31] H. Y. Wang, H. J. Mo and Y. P. Jing, *Environmental Dependence of Cold Dark Matter Halo Formation*, Mon. Not. Roy. Astron. Soc. **375** (2007) 633, doi:10.1111/j.1365-2966.2006.11316.x [arXiv:astro-ph/0608690 [astro-ph]].
- [32] F. Marinacci, M. Vogelsberger, R. Pakmor, P. Torrey, V. Springel, L. Hernquist, D. Nelson, R. Weinberger, A. Pillepich and J. Naiman, et al. *First results from the IllustrisTNG simulations: radio haloes and magnetic fields*, Mon. Not. Roy. Astron. Soc. **480** (2018) 5113, doi:10.1093/mnras/sty2206 [arXiv:1707.03396].
- [33] J. P. Naiman, et al. *First results from the IllustrisTNG simulations: a tale of two elements - chemical evolution of magnesium and europium.*, Mon. Not. Roy. Astron. Soc. **477** (2018) 1206, doi:10.1093/mnras/sty618 [arXiv:1707.03401].
- [34] D. Nelson, A. Pillepich, V. Springel, R. Weinberger, L. Hernquist, R. Pakmor, S. Genel, P. Torrey, M. Vogelsberger and G. Kauffmann, et al. *First results from the IllustrisTNG simulations: the galaxy colour bimodality*, Mon. Not. Roy. Astron. Soc. **475** (2018) 624, doi:10.1093/mnras/stx3040 [arXiv:1707.03395].
- [35] A. Pillepich, D. Nelson, L. Hernquist, V. Springel, R. Pakmor, P. Torrey, R. Weinberger, S. Genel, J. Naiman and F. Marinacci, et al., *First results from the IllustrisTNG simulations: the stellar mass content of groups and clusters of galaxies*, Mon. Not. Roy. Astron. Soc. **475** (2018) 648, doi:10.1093/mnras/stx3112 [arXiv:1707.03406].
- [36] V. Springel, R. Pakmor, A. Pillepich, R. Weinberger, D. Nelson, L. Hernquist, M. Vogelsberger, S. Genel, P. Torrey and F. Marinacci, et al. *First results from the IllustrisTNG simulations: matter and galaxy clustering*, Mon. Not. Roy. Astron. Soc. **475** (2018) 676, doi:10.1093/mnras/stx3304 [arXiv:1707.03397].



- [37] D. Nelson, V. Springel, A. Pillepich, V. Rodriguez-Gomez, P. Torrey, S. Genel, M. Vogelsberger, R. Pakmor, F. Marinacci and R. Weinberger, et al. *The IllustrisTNG Simulations: Public Data Release*, [arXiv:1812.05609].
- [38] R. Adam *et al.* [Planck], *Planck 2015 results. I. Overview of products and scientific results*, *Astron. Astrophys.* **594** (2016) A1, doi:10.1051/0004-6361/201527101 [arXiv:1502.01582 [astro-ph.CO]].
- [39] V. Springel, S. D. M. White, G. Tormen and G. Kauffmann, *Populating a cluster of galaxies. 1. Results at  $z = 0$* , *Mon. Not. Roy. Astron. Soc.* **328** (2001) 726, doi:10.1046/j.1365-8711.2001.04912.x [arXiv:astro-ph/0012055].
- [40] C. G. Lacey and S. Cole, *Merger rates in hierarchical models of galaxy formation*, *Mon. Not. Roy. Astron. Soc.* **262** (1993), 627
- [41] C. G. Lacey and S. Cole, *Merger rates in hierarchical models of galaxy formation. II. Comparison with  $N$  body simulations*, *Mon. Not. Roy. Astron. Soc.* **271** (1994), 676, doi:10.1093/mnras/271.3.676, [arXiv:astro-ph/9402069 [astro-ph]].
- [42] J. S. Bullock, A. Dekel, T. S. Kolatt, A. V. Kravtsov, A. A. Klypin, C. Porciani and J. R. Primack, *A Universal angular momentum profile for galactic halos*, *Astrophys. J.* **555** (2001), 240, doi:10.1086/321477 [arXiv:astro-ph/0011001 [astro-ph]].
- [43] A. V. Kravtsov and A. A. Klypin, *Origin and evolution of halo bias in linear and nonlinear regimes*, *Astrophys. J.* **520** (1999) 437, doi:10.1086/307495 [arXiv:astro-ph/9812311 [astro-ph]].
- [44] S. D. M. White, *Angular momentum growth in protogalaxies*, *Astrophys. J.* **286** (1984) 38, doi:10.1086/162573